

# *A global perspective on the upper branch of the Hadley Cell*

Article

Published Version

Creative Commons: Attribution 4.0 (CC-BY)

Open Access

Hoskins, B. J. and Yang, G. -Y. ORCID: <https://orcid.org/0000-0001-7450-3477> (2023) A global perspective on the upper branch of the Hadley Cell. *Journal of Climate*, 36 (19). pp. 6749-6762. ISSN 1520-0442 doi: <https://doi.org/10.1175/JCLI-D-22-0537.1> Available at <https://centaur.reading.ac.uk/112687/>

It is advisable to refer to the publisher's version if you intend to cite from the work. See [Guidance on citing](#).

To link to this article DOI: <http://dx.doi.org/10.1175/JCLI-D-22-0537.1>

Publisher: American Meteorological Society

All outputs in CentAUR are protected by Intellectual Property Rights law, including copyright law. Copyright and IPR is retained by the creators or other copyright holders. Terms and conditions for use of this material are defined in the [End User Agreement](#).

[www.reading.ac.uk/centaur](http://www.reading.ac.uk/centaur)

**CentAUR**

Central Archive at the University of Reading

Reading's research outputs online

# A Global Perspective on the Upper Branch of the Hadley Cell

B. J. HOSKINS<sup>a,b</sup> AND G.-Y. YANG<sup>a,c</sup>

<sup>a</sup> *Department of Meteorology, University of Reading, Reading, United Kingdom*

<sup>b</sup> *Grantham Institute—Climate Change and the Environment, Imperial College, London, United Kingdom*

<sup>c</sup> *Climate Directorate, National Centre for Atmospheric Science, University of Reading, Reading, United Kingdom*

(Manuscript received 15 July 2022, in final form 12 June 2023, accepted 20 June 2023)

**ABSTRACT:** The global perspective presented here is built on earlier papers discussing the dynamics of the upper branch of the Hadley cell in the two solstitial seasons. The role of the tropics is made explicit in a conceptual model that is presented and evaluated. The fluctuation of deep tropical convection in longitude and time is seen as crucial. The filamentary outflows from such convective events move westward and across the equator deep into the winter hemisphere. The horizontal tilt of the cross-equatorial flow implies a significant upper-tropospheric flux of westerly momentum from the winter tropics to the summer hemisphere. These properties are related to the cross-equatorial propagation of wave activity triggered by deep tropical convection in the summer hemisphere. The filaments carry with them near-equatorial values of absolute vorticity and potential vorticity. After turning anticyclonically, some filaments move eastward and poleward to the equatorial edge of the winter subtropical jet. There is strong evidence they can interact with the eddies on this jet and enhance their poleward westerly momentum flux. In the global perspective, tropical and extratropical systems and the interaction between them are all important for the dynamics of the upper branch of the Hadley cell.

**SIGNIFICANCE STATEMENT:** The Hadley cell is the large-scale overturning in the atmosphere with air in the upper troposphere moving from the equatorial region to near 30° in the winter hemisphere. In the standard view it is midlatitude weather systems that are responsible for removing angular momentum from this upper branch of the Hadley cell. Here it is proposed that tropical systems and their interaction with the midlatitude systems are also important. Insight into the role of the tropics in the dynamics of the Hadley cell can be obtained by considering it as the sum of many events of active deep convection occurring in different longitudes and at different times.

**KEYWORDS:** Atmospheric circulation; Atmospheric waves; Convection; Hadley circulation; Upper troposphere; Angular momentum


## 1. Introduction


The perspective on the Hadley cells developed in the seminal work of [Schneider \(1977\)](#) and [Held and Hou \(1980\)](#) was that a steady, zonally symmetric Hadley cell owes its existence to the gradient in solar heating in the tropics. In the lower branch, there were assumed to be weak easterly wind speeds and a balance between the Coriolis and frictional torques. In the upper branch angular momentum was assumed to be conserved, implying a subtropical jet speed of  $134 \text{ m s}^{-1}$  if the subtropical edge of the Hadley cell extends to latitude 30°.

[Schneider \(1977\)](#) viewed the Hadley cell produced in a zonally uniform tropical atmosphere as the basis for studying the growth and decay of extratropical eddies. The role of the momentum fluxes due to zonal asymmetries and temporal fluctuations in [Held and Hou \(1980\)](#) was merely to remove the

discontinuity in the westerly wind that would otherwise form at the subtropical edge of the Hadley cell. Subsequently, [Held \(2000, 2019\)](#), viewed baroclinic instability as providing the poleward limit on the extent of the Hadley cell, rather than the thermal wind and energy constraints applied in the earlier work. Many discussions of Hadley cells (e.g., [Schneider 2006](#); [Walker and Schneider 2006](#)) have been based on a zonally averaged perspective with extratropical weather systems considered as playing a dominant, controlling influence on the angular momentum distribution within the Hadley cells, as well as the nature and width of the cells. However, there has also been some recognition that a full theory would have to include some element of the impact of zonal asymmetries in the tropics.

The dominant behavior in the life cycle studies of baroclinic waves on jet flows on the sphere (e.g., [Simmons and Hoskins 1980](#); [Thorncroft et al. 1993](#)) is the production of strongly tilted troughs in the mature wave, followed by wave breaking and decay. The associated large poleward momentum transport extends equatorward, but not as deeply into the tropics as would be required if baroclinic waves were to be the mechanisms for removing westerly momentum from the deep tropical region. This conclusion is consistent with the first author's perusal of many synoptic maps on upper-tropospheric potential temperature surfaces. It is also consistent with the analysis of atmospheric data by [Randel and Held \(1991\)](#) who showed that poleward eddy momentum fluxes were significant only

 Denotes content that is immediately available upon publication as open access.

 Supplemental information related to this paper is available at the Journals Online website: <https://doi.org/10.1175/JCLI-D-22-0537.s1>.

Corresponding author: G.-Y. Yang, [g.y.yang@reading.ac.uk](mailto:g.y.yang@reading.ac.uk)

DOI: 10.1175/JCLI-D-22-0537.1

© 2023 American Meteorological Society. This published article is licensed under the terms of a Creative Commons Attribution 4.0 International (CC BY 4.0) License



poleward of the critical line on their equatorial flank. This implies that the existence of upper-tropospheric equatorial easterlies is crucial in limiting the equatorward extension of the extratropical eddy momentum flux.

The importance of the seasonal cycle, particularly the off-equatorial solar heating maximum in the solstitial seasons, was indicated by the results of the [Lindzen and Hou \(1988\)](#) extension of the [Held and Hou \(1980\)](#) model. The dominant solstitial Hadley cell has its ascent in the tropics of the summer hemisphere and descent in the winter subtropics. Angular momentum conservation in the upper branch gives easterlies on the equator and a winter subtropical jet that is reduced from the symmetric case, but still about twice that observed and with a discontinuity on its polar flank. As [Lindzen and Hou \(1988\)](#) comment, for realistic parameter values the cross-equatorial meridional wind away from the summer hemisphere is much weaker than that observed. However, together with equatorial easterlies this does imply a weak momentum transfer from the winter hemisphere to the summer hemisphere in this zonally symmetric model.

The upper-tropospheric angular momentum budget in the tropics and the existence of easterlies there has been the focus for several studies. Using 16 years of 200-hPa data, [Lee \(1999\)](#) showed that in the annual average the easterly acceleration in the equatorial region was predominantly given by the seasonal cycle of the Hadley cells. Her finding, that seasonal variations play an essential role in the annual angular momentum balance, was the motivation for the idealized modeling study of [Kraucunas and Hartmann \(2005\)](#). In this study with a symmetric, equinoctial basic state, a steady thermal source in the equatorial region is a source of poleward propagating Rossby waves, and therefore equatorward momentum transport, tending to drive equatorial westerlies. They concluded that the seasonal cycle and off-equatorial heating are crucial for the existence of equatorial easterlies in the upper troposphere.

[Dima et al. \(2005\)](#) used NCEP reanalysis data to examine the seasonal and zonal mean zonal momentum budget in the tropics. They found that in the upper troposphere in the equatorial region there is westerly acceleration due to the climatological stationary waves, primarily associated with Rossby wave generation, as in [Kraucunas and Hartmann \(2005\)](#). The westerly acceleration is balanced by the advection of easterly momentum associated with the cross-equatorial mean meridional circulation. As the accelerations are largest in the two solstitial seasons, the results were consistent with those of [Lee \(1999\)](#). [Dima et al. \(2005\)](#) also noted that the strength (and sign) of the eddy momentum flux in the deep tropics varies in concert with the seasonal cycle of the mean meridional flow across the equator.

[Grise and Thompson \(2012\)](#) found that enhanced equatorward momentum transport in the equatorial region is associated with large equatorial wave amplitude. They also noted that enhanced poleward momentum transport in the extratropics is associated with it, consistent with the results presented in [Kraucunas and Hartmann \(2005\)](#).

The aims of the present paper are to investigate the role of the tropical region in the dynamics of the upper branch of the Hadley cells and to show how both tropical and extratropical

systems contribute to the angular momentum and vorticity balance there. Further, features driven by deep convection in the tropics are found to be able to interact with eddies on the winter subtropical jet to produce enhanced poleward momentum transfer in the subtropics. The evidence that easterly winds in the tropical upper troposphere in the equatorial region owe their existence to the seasonal cycle and off-equatorial heating in the solstitial seasons suggests that more insight may be obtained by considering the winter seasons in the two hemispheres rather than the annual average. Consistent with this, the present paper builds on two previous papers on the June–August (JJA) and December–February (DJF) Hadley cells ([Hoskins et al. 2020](#), hereafter [HC<sub>JJA</sub>](#); [Hoskins and Yang 2021](#), hereafter [HC<sub>DJF</sub>](#)). In these papers, asymmetries in longitude and fluctuations in time in the tropics were found to be of order one importance for the dynamics of the upper branch of the winter Hadley cells.

Further analysis is given in this paper of the extent to which the conceptual view of the dynamics of the upper branch of the Hadley cell emerging from [HC<sub>JJA</sub>](#) and [HC<sub>DJF</sub>](#) is supported by reanalysis data. The analysis is mostly for the boreal summer, JJA, this season being chosen for several reasons:

- 1) In JJA there can be a focus on two main convective regions, the Indian Ocean (IO) and western Pacific (WP), as in [HC<sub>JJA</sub>](#). This contrasts with the DJF season for which it was found helpful in [HC<sub>DJF</sub>](#) to use many more regions of convection.
- 2) Zonal asymmetries are less important in the Southern Hemisphere, the winter hemisphere in JJA, than in the Northern Hemisphere in DJF. In particular, this is the case for the subtropical jet, which simplifies analysis of the influence on it of tropical convective flaring.
- 3) The impact of ENSO on the regions of tropical convection is generally at its smallest in JJA, and for this season it has been found that it is not necessary to stratify the data according to the phase of ENSO.

The organization of this paper is as follows. [Section 2](#) gives a summary of the data and equations used. [Section 3](#) builds on the dynamical results in [HC<sub>JJA</sub>](#) and [HC<sub>DJF</sub>](#), and introduces a conceptual model of the global Hadley cell in a solstitial season. In the following section, [section 4](#), the relationships between variables related to the conceptual model are investigated using joint pdfs, and the extent to which the model is supported is discussed. The relationship between the magnitude of the winter STJ and tropical convection is the topic of [section 5](#). This is followed, in [section 6](#), by a concluding discussion. Some indications of the robustness of the analysis in [sections 4](#) and [5](#) are given in the online supplemental material.

## 2. Data and equations used

Data used in this study are ECMWF ERA-Interim reanalysis horizontal winds ( $u$ ,  $v$ ) and vorticity, for the 30-yr period from 1981 to 2010. The fields are available 6-hourly with horizontal resolution of about  $0.7^\circ$  and at 37 pressure levels from 1000 to 1 hPa. Detailed information on the data can be found in [Dee et al. \(2011\)](#). As a proxy for the occurrence of deep tropical convection, use is made of NOAA interpolated daily

outgoing longwave radiation (OLR) (Liebmann and Smith 1996). This has a horizontal resolution of  $2.5^\circ \times 2.5^\circ$ .

To probe the observed relationship between variables (sketched in Fig. 2), joint pdfs between some of them will be shown. For the calculation of joint pdfs of dynamical variables with OLR, boxes  $10^\circ$  in longitude are used for all variables. For OLR the boxes are from  $0^\circ$  to  $20^\circ\text{N}$ , and daily OLR are averaged over this box. For the dynamical variables the boxes are  $5^\circ$  in latitude and centered every  $5^\circ$  from  $5^\circ$  to  $20^\circ\text{S}$ . The joint pdfs of the average values of OLR in its box and of all the daily average gridpoint values of dynamical variables in their boxes are accumulated in bins. The sizes of these bins and the ranges covered by the bins for the various variables discussed below are given in Table 1. The joint pdfs for a longitudinal region are produced by summing over those for the longitude boxes in that region.

Since the remote upper-tropospheric dynamical response to tropical convection is generally displaced to the west and lagged in time, various longitudinal and temporal displacements in space and time with respect to OLR have been considered for the dynamical variables. Little sensitivity is found to the values used, but generally smaller displacements give somewhat sharper relationships at very low latitudes, and larger displacements are better at higher latitudes. In section 4, the values shown are for the dynamical variables displaced  $10^\circ$  to the west and lagged 1 day in time with respect to OLR.

The only exception to this calculation method is the final joint pdf given in section 4, that for meridional wind and absolute vorticity. Since the main interest here is in the product of the two variables, the daily average of the values of both variables at the grid points in the boxes are binned directly.

A full discussion of the equations used was given in, for example, the appendix of HC<sub>JJA</sub>. Here, a summary of those equations directly relevant to this paper is given.

It is convenient to use  $\mu = \sin\phi$  as latitudinal coordinate, where  $\phi$  is the latitude, and  $U = u \cos\phi$ ,  $V = v \cos\phi$  as velocity variables. Then the specific absolute angular momentum is

$$A = a^2\Omega(1 - \mu^2) + aU, \quad (1)$$

where  $a$  is the radius of Earth, and  $\Omega$  is its rotation rate. The vertical component of absolute vorticity is

$$\zeta = 2\Omega\mu + \frac{1}{a(1 - \mu^2)} \frac{\partial V}{\partial \lambda} - \frac{1}{a} \frac{\partial U}{\partial \mu}. \quad (2)$$

In the zonal average, denoted by square brackets, the angular momentum and absolute vorticity are related:

$$\frac{1}{a} \frac{\partial [A]}{\partial \mu} = -a[\zeta]. \quad (3)$$

However, this is not true in a limited longitudinal sector, and the Lagrangian behavior of vorticity is much easier to consider because, unlike angular momentum, its rate of change is not directly influenced by pressure forces.

The zonally averaged (indicated by square brackets) and temporally averaged (indicated by a bar) angular momentum

TABLE 1. Bin characteristics for the variables in the joint pdfs. In each case there were no values in bins outside the specified range.

Variable	Units	Bin size	Range of bin centers
OLR	$\text{W m}^{-2}$	10	140 to 290
$V$	$\text{m s}^{-1}$	2	-44 to +52
$UV$	$\text{m}^2 \text{s}^{-2}$	40	-1960 to +1800
Absolute vorticity $\zeta$	$10^{-5} \text{s}^{-1}$	0.5	-23.5 to +10
$U$	$\text{m s}^{-1}$	5	-60 to +120

equation can be written in terms of meridional fluxes of westerly momentum:

$$0 = -\left[\frac{\partial}{\partial \mu}(UV)\right] - a\left[\frac{\partial}{\partial p}(\omega U)\right] + af[\bar{V}] + [\bar{F}], \quad (4)$$

$$0 = a[\bar{V}\zeta] - a\left[\omega \frac{\partial U}{\partial p}\right] + [\bar{F}]. \quad (5)$$

Here, the flux of absolute vorticity includes the Coriolis term and the flux of relative vorticity,  $\xi$ , and the two forms of the angular momentum equation are equivalent because

$$[V\xi] = -\frac{1}{a} \frac{\partial}{\partial \mu}[UV] - \left[U \frac{\partial \omega}{\partial p}\right]. \quad (6)$$

The zonal and temporal mean northward flux of any variable  $X$  can be analyzed using time averages  $\bar{()}$ , and deviations from them  $()'$ , and longitudinal averages  $[ ]$ , and deviations from them  $()^*$ :

$$[\bar{V}\bar{X}] = [\bar{V}][\bar{X}] + [\bar{V}'][\bar{X}'] + [\bar{V}^* \bar{X}^*] + [\bar{V}^{*'} \bar{X}^{*'}]. \quad (7)$$

The four terms on the right-hand side will, respectively, be referred to as the steady Hadley cell flux, the transient Hadley cell flux, the stationary eddy flux and the transient eddy flux. If only the temporal split is used, as in HC<sub>JJA</sub> and HC<sub>DJF</sub>, then the steady flux is composed of terms 1 and 3, the transient flux terms 2 and 4. If only the longitudinal split is used, then the Hadley cell flux is composed of term 1 and 2 and the eddy flux terms 3 and 4. Since the transient Hadley cell term, term 2, is found to be relatively very small when considering solstitial seasonal means, the main difference between analyses based on the two partial splits is whether term 3 is combined with term 1 or with term 4. The full analysis will be applied to the meridional flux of  $U$  and the absolute vorticity  $\zeta$ .

### 3. Extensions of previous results

Regressions of upper-tropospheric wind and absolute vorticity on OLR for convective regions in the summer tropics in the Indian Ocean and west Pacific and for JJA and DJF are shown in Fig. 1.<sup>1</sup> The JJA fields are for OLR in the Indian Ocean (IO) and west Pacific (WP) regions defined in HC<sub>JJA</sub>

<sup>1</sup> Previous results for the regression of wind fields on OLR were shown in Figs. 11 and 12 of HC<sub>JJA</sub> and Fig. 8a of HC<sub>DJF</sub>.



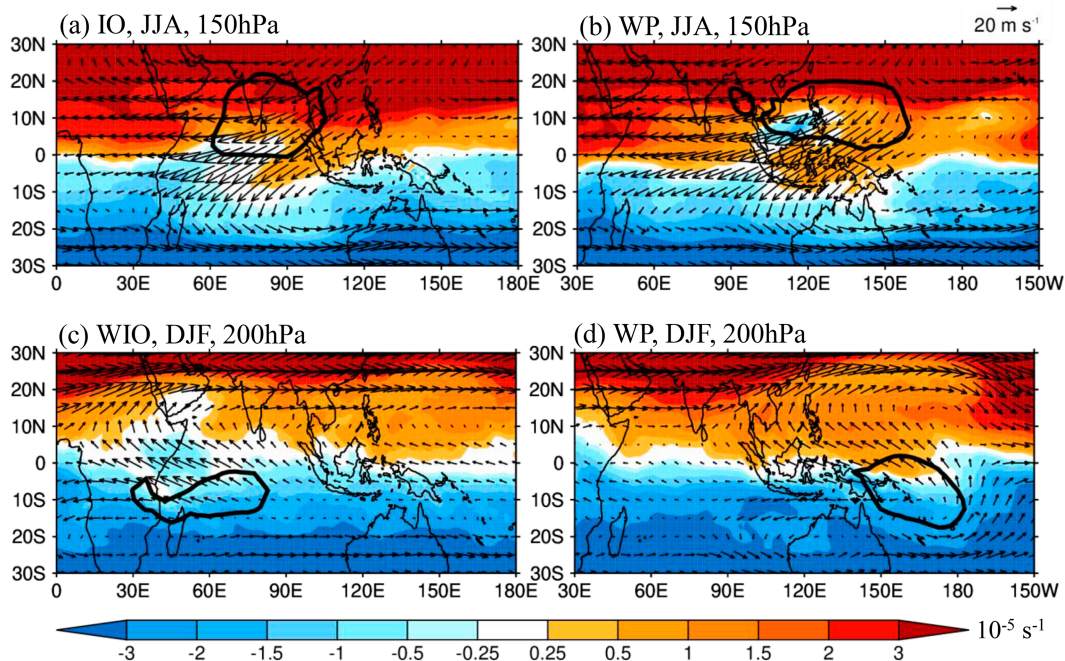


FIG. 1. (top) The 150-hPa wind vectors and absolute vorticity (color) regressed on OLR in (a) the Indian Ocean (IO) and (b) west Pacific (WP) regions for 30 years of JJA. (bottom) The 200-hPa wind vectors and absolute vorticity regressed on OLR in (c) the west Indian Ocean (WIO) and (d) western Pacific (WP) regions for 30 years of DJF. The regressed OLR of  $-175 \text{ W m}^{-2}$  is indicated by a thick black contour. The scales for the wind vectors are shown at the top right. The JJA IO and WP regions are defined in  $\text{HC}_{\text{JJA}}$  (their Fig. 4c), and the DJF WIO and WP regions are defined in  $\text{HC}_{\text{DJF}}$  (their Fig. 5c and their Table 1).

(their Fig. 4c). The DJF fields are for OLR in the West Indian Ocean (WIO) and west Pacific (WP) regions defined in  $\text{HC}_{\text{DJF}}$  (their Fig. 5c and their Table 1). In all cases active deep convection, as indicated by the low values of OLR inside the heavy black contour, is occurring predominantly in the region that was defined for the regression.

In the JJA cases (Figs. 1a,b) there are strong upper-tropospheric outflows from the region of deep convection with winds that are directed westward and across the equator into the Southern (winter) Hemisphere. The outflow turns in the region  $10^{\circ}$ – $15^{\circ}\text{S}$  and beyond this it becomes a southeastward flow toward the equatorial side of the winter subtropical jet (STJ). In both cases, contours of absolute vorticity are consistent with the cross-equatorial flow carrying Northern Hemisphere values into the Southern Hemisphere (the warm colors), and near equatorial values (light blue colors) being brought close to the STJ. Individual case studies shown in  $\text{HC}_{\text{DJF}}$  and  $\text{HC}_{\text{JJA}}$  indicate the filamentary nature of the outflow from the convective region. There is a suggestion in Figs. 1a and 1b that the extended outflow moves into the STJ region just ahead of a trough in it, and this is much clearer in individual case studies. The  $\pm 3$  day regressions given in Fig. 13 of  $\text{HC}_{\text{JJA}}$  show the progression of the filaments over the 6 day period from the regions of strong convection, turning anticyclonically and then interacting with the waves on the winter subtropical jet.

The outflows in the DJF cases (Figs. 1c,d) behave generally like the mirror image in the equator of those in JJA, directed westward and into the winter hemisphere, turning anticyclonically,

and carrying near equatorial values of absolute vorticity into the equatorial side of the winter STJ. As in JJA, this would be consistent with strengthening the winter STJ and influencing the waves on it.

The time scales that are important in the variability of the upper-tropospheric dynamics associated with active deep convection have been discussed in a number of previous papers [e.g., Yang et al. (2007a,b) and  $\text{HC}_{\text{JJA}}$  for JJA;  $\text{HC}_{\text{DJF}}$  for DJF]. Spectral peaks were found on synoptic time scales and on a week to intraseasonal time scales. However, regressions like those in Fig. 1 tend to emphasize the longer time scales.

Synoptic pictures of 370-K potential vorticity given in  $\text{HC}_{\text{JJA}}$  (their Fig. 14) and 350-K potential vorticity in  $\text{HC}_{\text{DJF}}$  (their Fig. 12) show in a more striking manner the filamentary nature of the outflows, the approximate conservation of potential vorticity in them, and their interaction with the STJs. This is the case in DJF as well as in JJA, despite the regression results in Fig. 1 for this season looking somewhat less impressive in this regard.

Based on results such as those shown here in Fig. 1, the discussion in  $\text{HC}_{\text{JJA}}$  and  $\text{HC}_{\text{DJF}}$ , and the material to be given below, a conceptual view of the essential ingredients for the upper branch of the solstitial Hadley cell is presented in Fig. 2. Here, the season is taken to be JJA, so that the Northern Hemisphere is in summer and the Southern Hemisphere in winter. Tropical convection is posed as flaring in summer hemisphere tropical regions at certain longitudes at certain times. The outflows from the convective events form filaments that

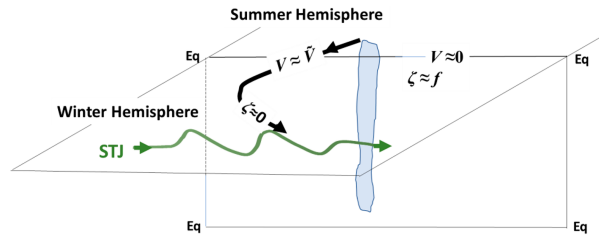


FIG. 2. An idealized conceptual view of the ingredients in the upper-tropospheric branch of the Hadley cell and their importance for fluxes of momentum and absolute vorticity  $\zeta$ . Filaments of air in the outflow from the top of active deep convection in the summer tropics move westward and across the equator into the winter tropics with a meridional wind component  $V$  of magnitude  $\bar{V}$ . The filaments carry with them very small values of absolute vorticity  $\zeta$  typical of the equatorial region. They turn anticyclonically, and move eastward and toward the winter STJ, often approaching it eastward of a trough in the waves on it. Where and when there is not active deep convection, the magnitude of the meridional wind is small and the absolute vorticity is more comparable with the Coriolis parameter, as indicated on the right-hand side of the picture.

extend westward and into the winter hemisphere. The filaments carry with them near-equatorial values of absolute vorticity  $\zeta$  and potential vorticity. The filaments continue to move poleward, approaching the equatorial edge of the winter subtropical jet (STJ). Consistent with their low-latitude value of absolute vorticity and therefore strong anticyclonic relative vorticity, these filaments turn anticyclonically near  $12^\circ$ – $15^\circ$  of latitude and their movement becomes eastward as well as poleward. Some interact with the eddies on the STJ, perhaps enhancing the poleward westerly momentum flux on their equatorial side and also the magnitude of these eddies. Importantly, the northeast–southwest tilt of the cross-equatorial flow implies an upper-tropospheric flux of westerly momentum from the winter tropics to the summer hemisphere.

Elsewhere in space and time in the summer tropics, convection is weak. In the winter hemisphere the meridional wind is small and the vorticity more like some undisturbed value, here taken to be close to the Coriolis parameter  $f$ .

In this conceptual picture, if active convection occurs in a fraction of the longitudes  $\alpha_\lambda$  and for a fraction of the time  $\alpha_t$ , then its frequency in space and time is  $\alpha = \alpha_\lambda \alpha_t$ . The meridional wind in the upper branch of the time-average Hadley cell would be  $\alpha$  times the value in an individual event, and the absolute vorticity would be  $f(1 - \alpha)$ . The speed of the STJ would be  $\alpha$  times the value that would be given by angular momentum conservation from the equator to the latitude of the jet. Therefore, a frequency of occurrence of deep tropical convection  $\alpha$  of about  $1/3$  would give the observed speed of  $40$ – $45 \text{ m s}^{-1}$  near latitude  $30^\circ$ . In this picture the strong relationship between the signs of the zonally averaged cross-equatorial wind and the momentum flux near the equator in the seasonal cycle noted by Dima et al. (2005) is directly understood as the result of averaging over the regions of active deep convection and the outflows from them.

The importance accorded to convective events is reminiscent of Riehl and Malkus (1958) who saw that energetic

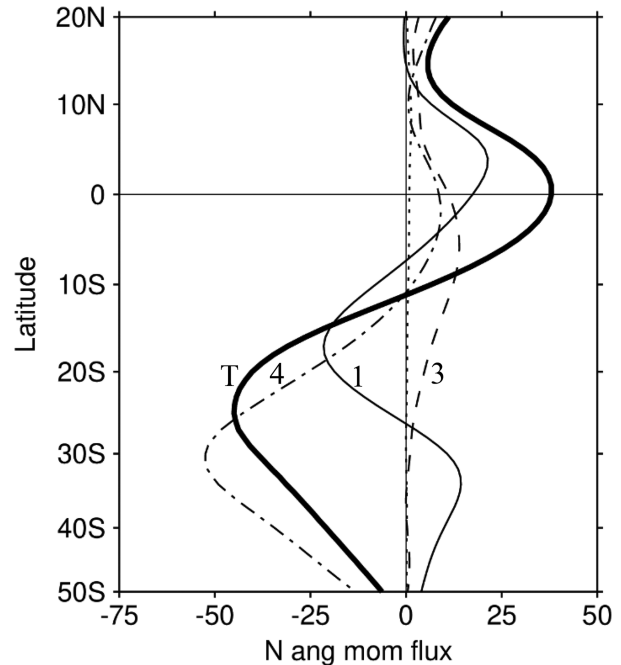


FIG. 3. The northward flux of angular momentum ( $\text{m}^2 \text{s}^{-2}$ ) for 30 years of JJA, as a function of latitude and averaged over the upper-tropospheric levels of 250, 200, and 150 hPa. The total flux (“T,” heavy solid line) and its split into the steady Hadley cell (“1,” solid line), transient Hadley cell (dotted line very close to the latitude-axis), stationary eddy (“3,” dashed line), and transient eddy (“4,” dash-dotted line) components as in Eq. (7).

constraints meant that the rising branch of the Hadley cell must be associated with active deep convection in “hot towers” rather than overall smooth ascent. The proposal here is that the motion toward the winter pole in the upper branch of the Hadley cell is best envisaged as arising from the outflow from these localized and intermittent regions of hot towers rather than as a uniform smooth flow.

The conceptual picture in Fig. 2 is highly idealized, showing a simple, extreme view in which either the meridional wind  $V$  is large and the absolute vorticity is near zero, or  $V$  is near zero and the absolute vorticity is not very different from that due to Earth’s rotation. In reality, some filaments outflowing from regions of active deep convection are absorbed in the subtropical “surf zone.” Associated with this, the background value of absolute vorticity in the regions without active deep convection is likely to be somewhere between  $f$  and zero.

It is also helpful to build on the discussion of the poleward fluxes of momentum and absolute vorticity in the previous papers. For brevity this will be done only for JJA and will be an extension of the analysis and discussion in HC<sub>JJA</sub> (illustrated there in Figs. 2 and 3). Figure 3a shows, as a function of latitude, the 30-yr JJA total northward flux of westerly momentum averaged over the upper-tropospheric levels 250, 200, and 150 hPa, and its split into its four components as in Eq. (7). The flux of momentum out of the region of the winter Hadley cell ( $0^\circ$ – $25^\circ\text{S}$ ) that is crucial for balancing the Coriolis torque there [see Eq. (4)] is performed by not only a poleward flux

maximizing near 25°S (value  $-45 \text{ m}^2 \text{ s}^{-2}$ ), but also by a cross-equatorial flux centered around the equator ( $38 \text{ m}^2 \text{ s}^{-2}$  at 1°N). Therefore, for the angular momentum that is removed from the upper branch of the Hadley cell, almost as much is transported across the equator into the tropics of the summer hemisphere as is transported toward the winter pole.

Looking at the component terms, the transient Hadley cell term (dotted) is negligible everywhere. The steady Hadley cell term is consistent with a direct mean circulation to 25°S and an indirect mean circulation (Ferrel cell) poleward of this, together with easterlies to 7°S and westerlies south of this. It and the stationary and transient eddy terms all contribute to the structure of the momentum flux from 5°N to 12°S. They are consistent with the northeast–southwest orientation of the outflows in Fig. 1 and the occurrence of these outflows occurring at some longitudes and at some times, and so with the conceptual model sketched in Fig. 2. Poleward of 20°S the stationary eddy term becomes small as expected in the Southern Hemisphere. The transient eddy term increases its negative value smoothly from 12°S to the latitude of the STJ and its contribution to the momentum flux dominates in the neighborhood of the jet. Following the view of Starr (1948) and collaborators, the poleward transient flux in the subtropics is often viewed as being purely due to troughs extending from transient eddies on the STJ. However, the smooth continuation of the transient flux from its maximum near the STJ into the tropics, compared with the subtropical limit to the momentum fluxes usually found in baroclinic waves (e.g., Simmons and Hoskins 1980) and expected from the critical line arguments of Randel and Held (1991) is suggestive that there may also be an interaction between the transients of extratropical and tropical origin, as first suggested by Riehl (1950).

Figure 4 shows the 30-yr JJA total northward flux of absolute vorticity, again as a function of latitude and averaged over the upper-tropospheric levels 250, 200, and 150 hPa. It also shows its components, as in Eq. (7).<sup>2</sup> In the form of the angular momentum budget given in Eq. (5), in the upper branch of the winter Hadley cell the frictional and vertical advection terms are expected to be small, and so the remaining term, the zonally and temporally averaged absolute vorticity flux, should be small. As seen in Fig. 4, this is indeed the case south of the equator because of large cancellations between the component terms. (In the region of deep convection, 0°–10°N, the cancellation is weak, and it is likely that vertical advection of momentum is important here.)

Looking at Fig. 4, the transient Hadley cell term (dotted) is seen to be negligible everywhere. The value that the steady Hadley cell flux would have if the relative vorticity were zero  $f[\bar{V}]$  is also plotted in Fig. 4. If angular momentum was conserved in zonally symmetric motion, this flux would be zero as the absolute vorticity would be zero. The actual steady Hadley cell flux is about halfway between these extremes. In the SH tropics, the cancellation of the steady Hadley cell flux is

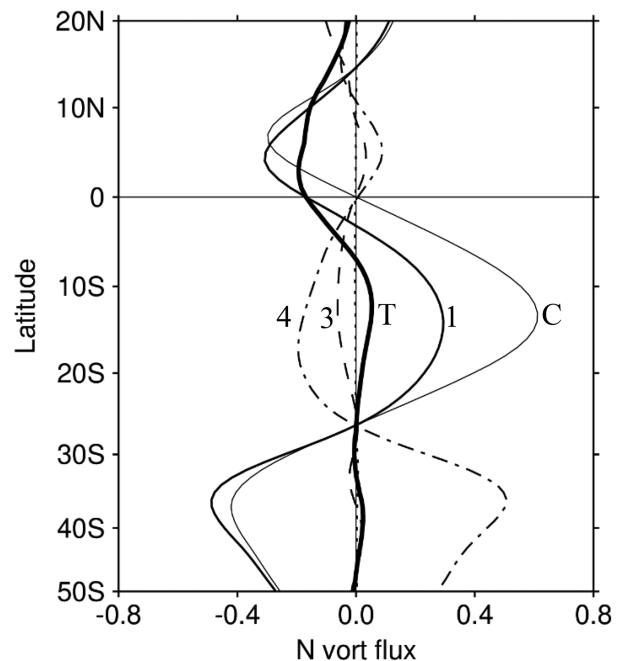


FIG. 4. The northward flux of absolute vorticity ( $1 \times 10^{-4} \text{ m s}^{-2}$ ) for 30 years of JJA as a function of latitude and averaged over the upper-tropospheric levels 250, 200, and 150 hPa. The total flux of absolute vorticity (“T,” heavy solid line) and its split into the Coriolis term (“C,” thin solid line), mean Hadley cell (“1,” solid line), transient Hadley cell (dotted line very close to the latitude axis), stationary eddy (“3,” dashed line), and transient eddy (“4,” dash-dotted line) components as in Eq. (7).

by the eddy fluxes, with the transient eddy flux larger than the stationary eddy flux. Poleward of 27°S, the reversed steady flux is balanced almost completely by the positive transient eddy flux. From Eq. (6), given the likely small magnitude of the term involving  $\omega$  on these scales, the southward eddy vorticity fluxes peaking near 12°S are consistent with the momentum fluxes out of this region shown in Fig. 3.

The near zero magnitude of the total absolute vorticity flux in the upper branch of the winter Hadley cell, and the importance of the steady Hadley cell flux, and also of the stationary and transient eddy fluxes of both momentum and vorticity are consistent with the conceptual model illustrated in Fig. 2.

#### 4. Analysis of relationships between the variables

In this section the relationships in the 30-yr period between variables that are involved in the conceptual picture, Fig. 2, will be investigated through joint pdfs of daily averages of the variables. The method for calculating the joint pdfs was detailed in section 2. Here results will be shown for the latitude circle (LC), and for the Western and Eastern Hemispheres (WH and EH, respectively). The results for more limited longitudinal sectors in WP and IO have been analyzed but were not significantly different from those for the larger EH region containing them. From Figs. 1 and 2, any characteristic behavior in the upper-tropospheric dynamical variables in the

<sup>2</sup> A similar picture, but for a single level, for one year only and with a reduced breakdown into components, was given in Fig. 3 of HC<sub>JJA</sub>.

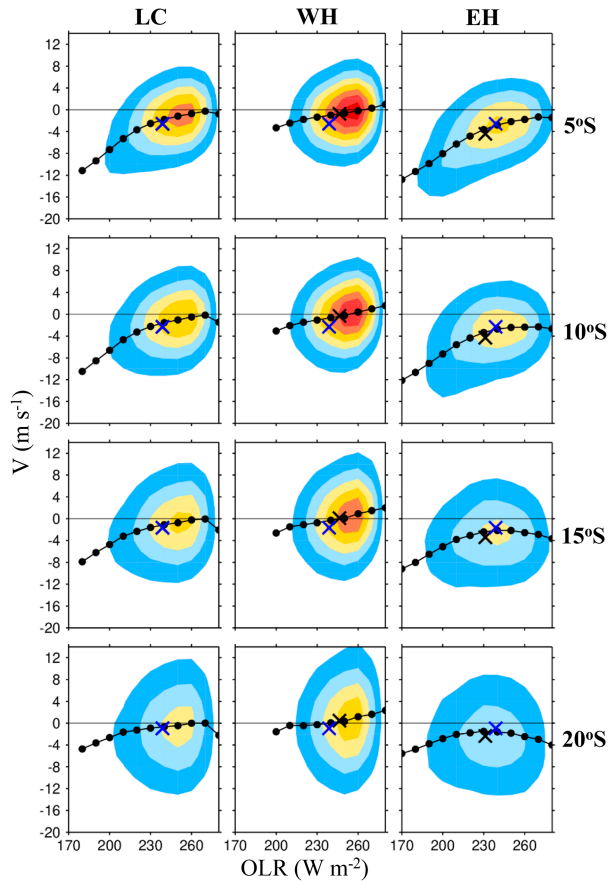


FIG. 5. Joint pdfs of daily OLR (abscissa) and  $V$  (ordinate). The pdfs for the (left) latitude circle (LC), (center) Western Hemisphere (WH), and (right) Eastern Hemisphere (EH). The rows are for  $5^\circ$ ,  $10^\circ$ ,  $15^\circ$ , and  $20^\circ$ S. Boxes  $10^\circ$  in longitude are used for both variables. For OLR the boxes are all from  $0^\circ$  to  $20^\circ$ N, and daily OLR values are averaged over them. For the dynamical variables the boxes are  $5^\circ$  in latitude and centered every  $5^\circ$  from  $5^\circ$  to  $20^\circ$ S, and each is shifted  $10^\circ$  to the west of the corresponding OLR box and the values are lagged one day in time. The daily joint pdfs of the average values of OLR in its box and all the gridpoint values of dynamical variables in their box are accumulated in bins to give the joint pdf. The contour interval is uniform. The blue crosses are the average values of the variables over all longitudinal grid points, and the black crosses are the longitudinal average in the sector. The black dots joined by a line indicate the average value of the dynamical variable for each OLR bin. They are shown only when more than 1% of the data is contained within the OLR bin.

winter hemisphere associated with the flaring of summer hemisphere tropical convection, and the associated low values of OLR, can generally be expected to occur in a region shifted to the west and lagged in time compared with it. The results for dynamical variables with westward spatial shifts of  $0^\circ$  and  $10^\circ$  in longitude and time lags of 0, 1 and 2 days with respect to the tropical OLR are all found to be quite similar. In general, a  $10^\circ$  longitude westward shift and 1-day time lag for dynamical variables give slightly sharper results in the higher latitudes and will be used here.

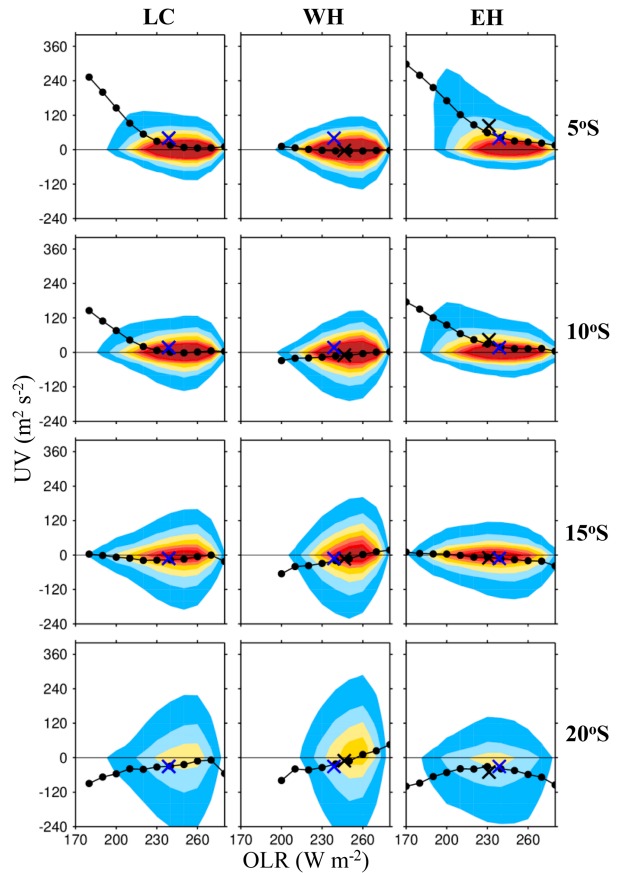


FIG. 6. Joint pdfs of daily OLR (abscissa) and total northward flux of westerly momentum  $UV$  (ordinate). The columns are for the LC, WH, and EH, and the rows are for  $5^\circ$ ,  $10^\circ$ ,  $15^\circ$ , and  $20^\circ$ S. The conventions and details are as in Fig. 5.

The joint pdfs of OLR in the  $0^\circ$ – $20^\circ$ N region, and the 150-hPa values of  $V$ ,  $UV$ , and the absolute vorticity  $\zeta$  every  $5^\circ$  from  $5^\circ$  to  $20^\circ$ S will be shown in Figs. 5–7 and discussed first. In each panel, the longitudinal and time average using only the bin values in the region will be indicated by a black cross. The average values of the dynamical variable as a function of OLR will be indicated by a sequence of black dots (one for each OLR bin) joined by a line. The blue cross indicates the average values of the variables computed using all longitudinal grid points and all values of the variables (not just those within the ranges of the bins used).

Figure 5 gives results for OLR (abscissa) and  $V$  (ordinate) and therefore on the relationship between the occurrence of convection in the summer hemisphere tropics and the upper-tropospheric meridional motion in the winter hemisphere. The latitude circle pictures (LC, column 1) exhibit considerable spread around the average Hadley cell values. The average value of  $0^\circ$ – $20^\circ$ N OLR is about  $239 \text{ W m}^{-2}$ . The average values, indicated by the black and blue crosses, are coincident within the errors associated with a limited range of the bins used for accumulating values. For OLR greater than about  $240 \text{ W m}^{-2}$ , the occurrence of deep convection is probably



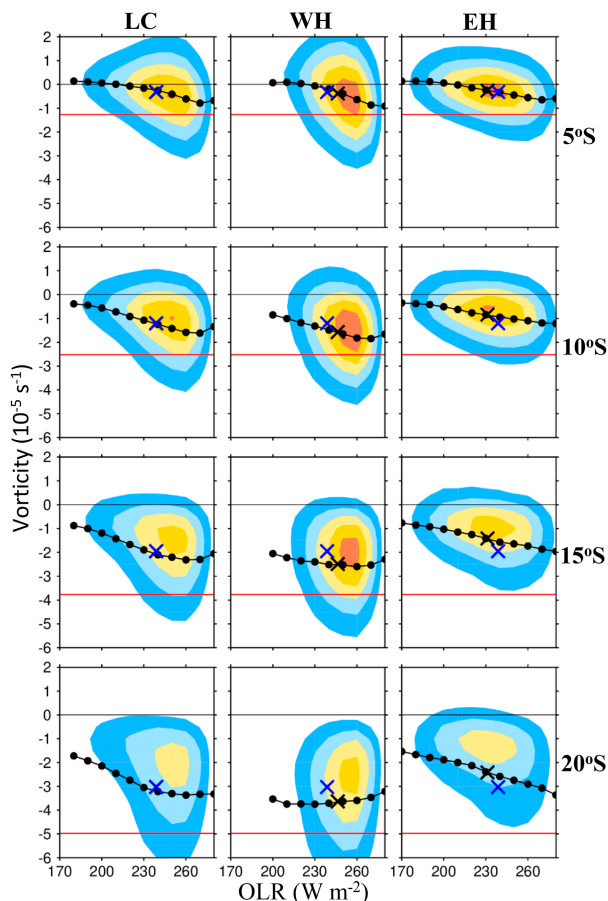


FIG. 7. Joint pdfs of daily OLR (abscissa) and absolute vorticity  $\zeta$  (ordinate). The columns are for the LC, WH, and EH, and the rows are for 5°, 10°, 15°, and 20°S. The horizontal red lines in each panel indicate the value of the Coriolis parameter at the central latitude. The conventions and details are as in Fig. 5.

limited in occurrence, and the maximum in the pdf and the average values for each  $10 \text{ W m}^{-2}$  OLR bin (black dots) is at, or near, zero  $V$ . For OLR values below about  $240 \text{ W m}^{-2}$ , the poleward motion increases with decreasing OLR and therefore with increasing deep tropical convective activity. It is striking that this is found even as far as 20°S, despite the application everywhere of a single choice of westward shift and time lag.

TABLE 2. Average values of  $UV$  ( $\text{m}^2 \text{ s}^{-2}$ ) in 5° Southern Hemisphere latitude bands centered from 5° to 20°S for all OLR (All), and for the 45% of data points with OLR below the average value of OLR,  $239 \text{ W m}^{-2}$ , and for the 55% of data points with OLR above this average value. The OLR values are computed using the averages of daily OLR in boxes of  $10^\circ$  in longitude and  $0^\circ$ – $20^\circ$ N. The  $UV$  values are averages of accumulated products of daily average gridpoint values of  $U$  and  $V$  for boxes that are  $10^\circ$  in longitude and  $5^\circ$  in latitude. This box for  $UV$  is shifted westward by  $10^\circ$  in longitude from that for OLR, and the values used are for a time lagged by one day compared with that for OLR.

OLR range	$UV$ at 5°S	$UV$ at 10°S	$UV$ at 15°S	$UV$ at 20°S
All	40	17	−12	−30
Below $239 \text{ W m}^{-2}$ (45%)	80	37	−14	−43
Above $239 \text{ W m}^{-2}$ (55%)	8	1	−10	−20

The pdfs for WH and EH are given in columns 2 and 3 of Fig. 5. As was the case for the LC, both show considerable spread in their pdfs. There is generally less deep convection in the WH. Consistent with this, the distributions at all latitudes in the less convective WH are weighted toward OLR values above  $240 \text{ W m}^{-2}$ , as shown by the maxima in the pdfs and by the averages shown by the black crosses. As with LC, these values of OLR are generally associated with small values of  $V$ . However, OLR values below  $240 \text{ W m}^{-2}$  do occur, and these are, on average, associated with increasingly negative values of  $V$ . The EH shows a range of OLR values but as shown by the black crosses, the average OLR and  $V$  values are lower than those for the zonal average (the blue crosses). As was the case for LC, on average at all latitudes there is little dependence of  $V$  on OLR for values greater than  $240 \text{ W m}^{-2}$  and an almost linear relation for values less than  $240 \text{ W m}^{-2}$ . In WH, from 10° to 20°S there are signs of a reversed Hadley cell motion ( $V > 0$ ) at high OLR values. This reversal could be analogous to the descent often found between deep convective towers in the ascending branch of the Hadley cell.

To give more information on the dependence of northward westerly momentum fluxes in the SH on deep convection in the northern tropics, joint pdfs for OLR and  $UV$  are shown in Fig. 6 with the same format as used in Fig. 5. Looking first at LC (column 1), the average values (crosses) are consistent with the total flux shown in Fig. 3, being positive at 5° and 10°S, and negative at 20°S. However, it is clear that a disproportionate share of the momentum fluxes is contributed by the grid points that have the lowest OLR values.

Table 2 gives the average values of  $UV$  for the four latitude ranges. It also gives the average values of  $UV$  for the 45% of data points with generally strong/active deep convection (OLR less than its average value) and for the 55% of points with generally weak/inactive deep convection (OLR greater than its average value). For the active convection category at 5° and 10°S the northward weak momentum transport contributes 90% and 98%, respectively, of the total. This is consistent with the Fig. 2 schematic with the outflow from deep convection moving in a NE–SW direction, and with the important cross-equatorial transport of momentum out of the upper branch of the Hadley cell being associated with this.

The averages for OLR bins (black dots) in column 1 of Fig. 6 show that the momentum transport increases smoothly for OLR decreasing below about  $240 \text{ W m}^{-2}$ . The latitude 15°S is close to the reversal latitude for the momentum



transport. At 20°S, the variation in tropical convective activity still has a significant impact. Locations and days with active tropical convection contribute almost 2/3 of the total momentum transport. This is despite this latitude being 30° south of the center of the tropical OLR region. This finding is consistent with the constructive interaction of the tropics with extratropical weather systems indicated in the conceptual model in Fig. 2 and seen in the synoptic examples in HC<sub>JJA</sub> and HC<sub>DJF</sub> and in Fig. 1.

The exact value of the westward shift and time lag that should be used for  $UV$  compared with OLR is not clear. It has been found that the change in the values of  $UV$  for OLR below and above its average value given in Table 2 is negligible if the time lag is not used for  $UV$  values. However, not using the westward shift gives a reduction in the dependence on OLR, particularly at higher latitudes. For example, using a lag of 1 day but no shift in longitude, the numerical values of  $UV$  for below and above 239  $W m^{-2}$  at 5°S change from the Table 2 values of 80 and 8, respectively, to 71 and 16, and at 20°S the values change from -43 and -20 to -35 and -27 without a shift. This is consistent with Figs. 1 and 2 and the winter hemisphere paths of the filaments from the outflows of summer tropical regions of deep convection generally being to the west of the convection.

Looking at WH and EH in Fig. 6 (columns 2 and 3), the enhanced momentum transport at 5° and 10°S for small OLR is seen to arise almost completely from the more convective EH. The signal of this is particularly strong in the IO region (not shown) and is like that for the whole EH in the WP region (not shown). At 20°S the contribution to the negative momentum transport is again predominantly from the lower OLR values in the EH, but this behavior is not as marked as at lower latitudes.

An important aspect of the discussion in this paper is the extent to which poleward-moving air that may be associated with the outflow from tropical convection exhibits near equatorial values of absolute vorticity, whereas elsewhere this is not the case. To examine this, joint pdfs of OLR and absolute vorticity are presented in Fig. 7. The LC pictures (column 1) at all the latitudes show that for OLR less than about 240  $W m^{-2}$  the absolute vorticity is indeed generally much closer to zero than to the value of the local Coriolis parameter (indicated by horizontal red lines). The absolute vorticity becomes closer to zero with decreasing values of OLR, indicative of more active deep convection. For OLR greater than 240  $W m^{-2}$ , implying generally inactive deep convection, there is a large spread in the values of absolute vorticity, mostly in the range from zero to the local Coriolis parameter. The WH is dominated by the higher OLR values. However, down to 15°S even in this hemisphere, when convection is active the typical magnitude of the absolute vorticity is smaller than when it is inactive. In the EH both behaviors are seen, with active convection being more prominent.

In Figs. 5–7, the difference between the WH and EH average values of OLR,  $V$ ,  $UV$ , and  $\zeta$  (black crosses) is consistent with deep convection and strong southward flow occurring together primarily in certain longitudinal regions. It is also consistent with the importance of the stationary eddy fluxes of

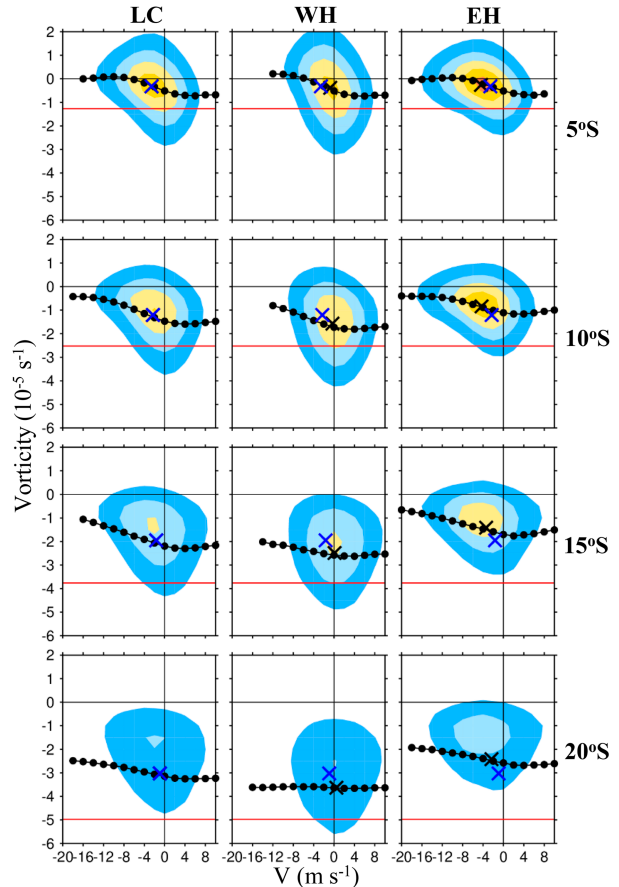


FIG. 8. Joint pdfs of daily  $V$  (abscissa) and absolute vorticity  $\zeta$  (ordinate). The columns are for the LC, WH, and EH, and the rows are for 5°, 10°, 15°, and 20°S. The data for the two variables are taken from the values at the same grid point and time. The black dots joined by a line indicate the average value of  $\zeta$  for each  $V$  bin. In each panel, the horizontal red line indicates the value of the Coriolis parameter at the central latitude. The other conventions and details are as in Fig. 5.

momentum and vorticity. The behavior of the average values of  $V$ ,  $UV$ , and  $\zeta$  as a function of OLR (black dots joined by lines) in Figs. 5–7, particularly for EH, are consistent with deep convection and strong southward flow occurring together primarily at certain times, and with the importance of the transient eddy fluxes.

Motivated by the requirement that the magnitude of the absolute vorticity flux,  $V\zeta$ , be small, the final joint pdf to be considered in this section is for  $V$  (abscissa) and absolute vorticity  $\zeta$  (ordinate) evaluated in the same boxes and at the same time. The daily average values of the two variables are recorded at every 1° grid point in longitude and latitude and accumulated over the specified region. The resulting joint pdfs, shown in Fig. 8, have a similar structure to those given in Fig. 7 for OLR and  $\zeta$ . Considering first the LC pdf, (column 1), for positive and small negative values of  $V$  there are a wide range of  $\zeta$  values, generally from slightly positive to slightly more negative than the local Coriolis parameter (indicated by

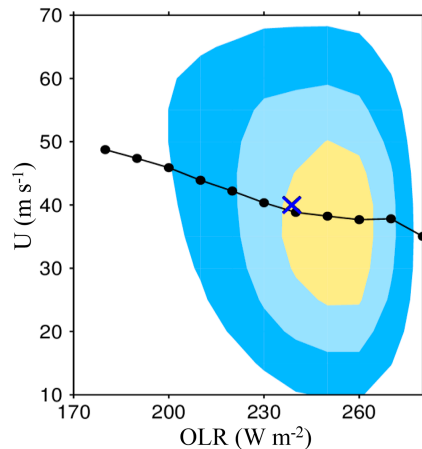


FIG. 9. Joint pdf of daily OLR (abscissa) and 3-day lagged  $U_{200-250}$  at  $30^\circ\text{S}$  (ordinate), for the LC. The black dots joined by a line indicate the average value of  $U$  for each OLR bin. The other conventions and details are as in Fig. 5.

horizontal red lines). For negative  $V$ , the ranges of  $\zeta$  values are generally narrower and for larger amplitudes in  $V$  become increasingly centered around smaller magnitudes in  $\zeta$ . For  $5^\circ\text{S}$  the central magnitudes for large negative  $V$  are very close to zero, and they are close to zero at both  $10^\circ$  and  $15^\circ\text{S}$ .

At all latitudes the small value of  $[\bar{V}\zeta]$  can be seen as resulting from the structure of the joint pdf, with small magnitudes in  $\zeta$  generally being associated with large magnitudes in  $V$ . Consistent with the discussion of the other joint pdfs, the small positive  $V$  behavior is predominant in the WH (column 2), whereas the large magnitude  $V$  and small  $\zeta$  behavior is more evident in the EH (column 3).

Tests have been performed to assess the dependence of the joint pdfs on interannual variability and on the climatological seasonal cycle. Figures 5–8 have been recomputed for variables in which the seasonal mean for each year has been replaced by the climatological value. The resulting changes (not shown) are very small. In a further test, the climatological seasonal cycle (represented by the first 12 harmonics) has also been removed from each variable. The results for the joint pdfs for the latitude circle are shown in the supplementary material (see Fig. S1). The variation in OLR is smaller but, as summarized in the black dots and curves, the behavior as a function of the ordinate is very similar. In addition, the robustness of the curves joining the black dots in Figs. 5–8 (and Fig. S1) is indicated by their smoothness despite the individual points being computed independently.

## 5. The relationship with the strength of the winter subtropical jet

Figure 6 indicates that, as far southward as  $20^\circ\text{S}$ , local momentum fluxes are influenced by Northern Hemisphere tropical convective activity in a similar, but slightly eastward-shifted, longitudinal region. Together with the regression results in Fig. 1, this is suggestive that there may be an effect on the strength of the STJ near  $30^\circ\text{S}$ . This Section gives the results of a limited

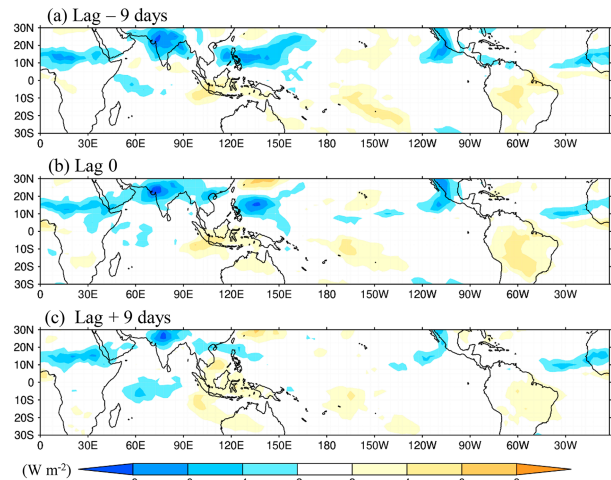


FIG. 10. Regressions of the anomaly in OLR (color, with contours as on the bar below) on the anomaly in the zonal average of  $U_{200-250}$  at  $30^\circ\text{S}$ . The OLR anomalies are for (a) 9 days before peak  $U$ , (b) at peak  $U$ , and (c) 9 days after peak  $U$ . The domain shown is from  $30^\circ\text{S}$  to  $30^\circ\text{N}$ .

analysis of the relationship between active deep tropical convection and the strength of the STJ as measured by the strength of the 200–250-hPa westerly wind  $U_{200-250}$  at  $30^\circ\text{S}$ .

The joint pdf of  $0^\circ$ – $20^\circ\text{N}$  OLR and  $U_{200-250}$  at  $30^\circ\text{S}$  is shown in Fig. 9. Here, a zero shift in longitude and a 3-day lag have been used, consistent with the regression examples shown in Fig. 1 and in HC<sub>JJA</sub>. This means that the values of the daily OLR are averaged over boxes covering  $0^\circ$ – $20^\circ\text{N}$  and  $10^\circ$  in longitude, and those of  $U_{200-250}$  three days later are averaged over boxes from  $28^\circ$  to  $32^\circ\text{S}$  in latitude and with the same longitudinal range. The values are accumulated in bins for all the days and around the latitude circle. As would be expected, there is a considerable range of winds for a given value of OLR. However, active convection/low OLR (OLR below  $240 \text{ W m}^{-2}$ ) biases the distribution and leads, on average, to stronger STJ winds 3 days later in the same longitude. This is despite there being a separation of some  $40^\circ$  of latitude between the two variables. For OLR greater than  $240 \text{ W m}^{-2}$  there is no such relationship. Analysis indicates that the pattern of the joint pdf is not sensitive to small changes in the lags and shifts chosen.

Another perspective on the relationship between tropical OLR and winter STJ wind strength is given by considering lagged regressions of OLR anomaly on to  $U_{200-250}$  at  $30^\circ\text{S}$  averaged either over the latitude circle or over  $60^\circ$  sectors. In each case lag  $-9$  will refer to the use of the OLR anomaly 9 days before peak  $U$ , lag 0 the simultaneous OLR anomaly, and lag  $+9$  the OLR anomaly 9 days after peak  $U$ . Figure 10 shows the OLR regression pictures for zonally averaged  $U_{200-250}$ . Some weak features, such as the negative OLR anomaly in West Africa, and Central America, and the positive anomaly OLR anomaly over the Maritime Continent, SPCZ, and South America change little during the 18 day period and, as will be discussed below, are associated with the annual cycle. The main features of interest are the negative OLR anomalies

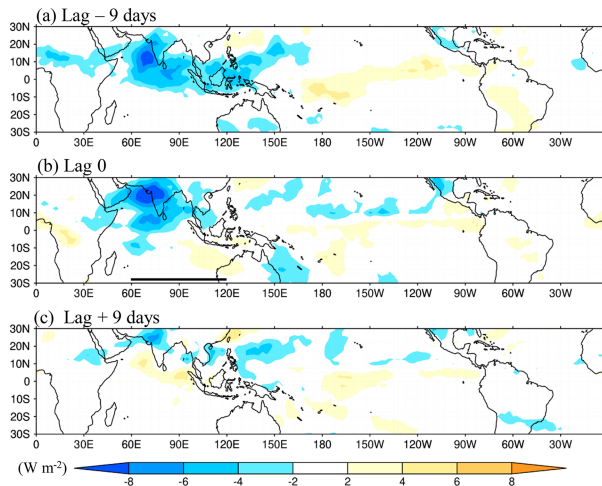


FIG. 11. (a)–(c) Regressions of the anomaly in OLR (color) on to the anomaly in the average of  $U_{200-250}$  at  $30^\circ\text{S}$  in the  $60^\circ\text{--}120^\circ\text{E}$  sector, which is indicated by a bold line in (b). The OLR anomalies are for (a) 9 days before peak  $U$ , (b) at peak  $U$ , and (c) 9 days after peak  $U$ .

in the South Asian and west Pacific regions that are strong for the OLR leading and simultaneous periods (Figs. 10a,b) but weaken for the OLR lagging (Fig. 10c). The OLR anomaly over India moves poleward during the period, which could be an intraseasonal oscillation (ISO) signature.

Figure 10 indicates that tropical Northern Hemisphere convective activity in the South Asian and west Pacific regions (encapsulated in the IO and WP regions in  $HC_{JJA}$ ) does tend to precede a strong zonally averaged Southern Hemisphere STJ.

Guided by the regressions in Fig. 1, the same pictures as in Fig. 10, but for  $U_{200-250}$  averaged over the longitude sectors  $60^\circ\text{--}120^\circ\text{E}$  and  $120^\circ\text{E--}180^\circ$  are shown in Figs. 11 and 12, respectively. For the Indian Ocean sector (Fig. 11) at lag  $-9$  days there tends to be reduced OLR from the Indian Ocean to the west Pacific. By lag 0 the west Pacific anomaly is no longer present, and the Indian Ocean anomaly has moved northward into South Asia. For lag  $+9$  days the OLR anomalies are weak. For the  $120^\circ\text{E--}180^\circ$  sector (Fig. 12) at lag  $-9$  days there are negative OLR anomalies over India and the west Pacific. By lag 0 both anomalies have shrunk in extent and the Indian anomaly has moved poleward. By lag  $+9$  days there are positive OLR anomalies in the Indian Ocean to the Maritime Continent, the Indian negative anomaly is no longer present, and the west Pacific anomaly has reduced and moved poleward.

The impacts of the Indian Ocean and west Pacific OLR anomalies on the STJ are not completely separated by considering the two adjacent  $60^\circ$  sectors for  $U$ , but each is dominant in one of them. For  $U$  averaged over the other  $60^\circ$  longitude sectors the OLR anomalies are much weaker and less organized than those shown here, except that for the sector  $0^\circ\text{--}60^\circ\text{E}$  in which there is an Indian Ocean OLR anomaly signal that is similar to, but weaker than, that for the sector to its east.

As for the joint pdfs, the regression analyses in this section have been repeated for variables with the seasonal mean and

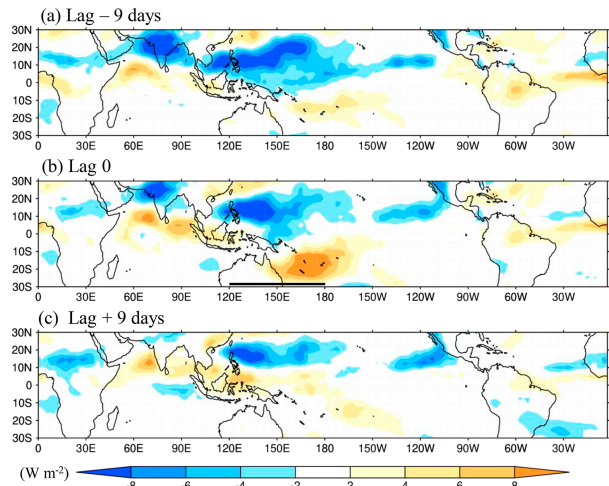


FIG. 12. (a)–(c) Regressions of the anomaly in OLR (color) on to the anomaly in the average of  $U_{200-250}$  at  $30^\circ\text{S}$  in the  $120^\circ\text{E--}180^\circ$  sector, which is indicated by a bold line in (b). The OLR anomalies are for (a) 9 days before peak  $U$ , (b) at peak  $U$ , and (c) 9 days after peak  $U$ .

annual cycle removed. Figure S2 shows the lag 0 results for zonal mean  $U_{200-250}$  and for its average in the two sectors. Comparing with the corresponding panels in Figs. 10–12, it is seen that the subseasonal time-scale phenomena must dominate in the observed relationships. The main difference is that the weak OLR features that changed little from lag  $-9$  days to lag  $+9$  days are largely removed.

The hypothesis that active Northern Hemisphere tropical convection in the South Asian and west Pacific regions is followed, on average, by a stronger local STJ is supported by the figures shown in this section. As expected, in these regression results using 30 years of data, the longer time scales of the ISO tend to dominate over synoptic time scales.

## 6. Conclusions

The results presented in this paper provide evidence that the outflow from active deep convection in the tropical summer hemisphere influences the dynamics of the upper troposphere in the winter hemisphere as far as the subtropical jet stream through cross-equatorial transports of absolute vorticity and angular momentum in thin filaments. To our knowledge, this is the first example of interhemispheric coupling of nonseasonal variability in the upper-tropospheric general circulation, apart from that in equatorially symmetric patterns as in ENSO and the MJO. It is clearly apparent in the climatological mean JJA circulation over the Indian Ocean and western Pacific sectors, and in the transients in both solstitial seasons. The zonal and time averaged flow from the tropics in the summer hemisphere to the winter hemisphere in the upper branches of the solstitial Hadley cells takes place largely within these filaments.

The evidence presented has supported the relevance of the conceptual model presented in Fig. 2. Each of the joint pdfs shown in Figs. 5–7 do not exhibit the bipolar structure that

the model would suggest if taken literally. However, it has been convenient to frame the discussion of them in terms of the behavior for increasingly active deep convection and for weak or no convection, with an OLR value of  $240 \text{ W m}^{-2}$  acting as approximate boundary between the two regimes. Consistent with this, the pdfs can be viewed as the sum of two simpler distributions, one for a range of active convection and one for weak or no convection. Evidence in support of the conceptual model has here been obtained for the JJA season, but the results given in  $\text{HC}_{\text{DJF}}$  are supportive of its value also for this solstitial season. In DJF, there are few mobile, transient eddies on the STJ in the longitudes of the main convective regions, and  $\text{HC}_{\text{DJF}}$  shows evidence in Figs. 8, 9, and 12 of tropical filaments interacting more directly with the strong Rossby waveguide formed by the African–Asian STJ. This can be expected to influence the behavior of eddies downstream in the North Pacific storm track. In equinoctial seasons it is envisaged that the filaments from the tops of deep convection on either side of the equator move westward and across the equator toward the subtropics of the other hemisphere.

Two departures from the standard picture of the transport of angular momentum out of the region of the upper branch of the Hadley cell are highlighted here. The first is that in the solstitial seasons the eddy transport across the equator into the summer hemisphere is very important. From the data that is illustrated in Fig. 3, in JJA some 46% of the transport of angular momentum out of the 100–250-hPa layer and the region from  $25^{\circ}\text{S}$  to  $1^{\circ}\text{N}$  is into the summer hemisphere (Its convergence there balances the Coriolis torque on the Hadley cell flow from the latitude of maximum deep convection toward the equator.) Dima et al. (2005) noted that eddy momentum flux in the deep tropics varies through the year in concert with the cross-equatorial motion. In the perspective presented in this paper this link is self-evident because they are both directly related to the motion of the filaments of air in the outflows from active convective regions. This cross-equatorial momentum transport, changing sign from one solstitial season was apparent in the first general circulation diagnostics atlas based on ECMWF global analyses (Hoskins et al. 1989).

The intention of this paper is not the investigation of the vertically integrated angular momentum budget for the winter tropics. However, it is apparent from Fig. 2 in  $\text{HC}_{\text{JJA}}$  and Fig. 2 in  $\text{HC}_{\text{DJF}}$ , that in the vertical average, the transport of angular momentum out of the region into the extratropics is some 2–3 times larger than that across the equator, because of the relative confining of the latter to the upper troposphere. In fact, in DJF there is a smaller reverse transport in the 600–850-hPa layer into the Northern (winter) Hemisphere associated with the cross-equatorial flow from the top of the shallow Northern Hemisphere oceanic ITCZ into the Southern Hemisphere latitude of the rising branch of the Hadley cell.

The second departure from the standard picture is related to the poleward transport of angular momentum from the upper branch of the Hadley cell. From as far equatorward as  $15^{\circ}$  in the winter hemisphere this is usually associated purely with extratropical waves, but here it is proposed that a portion of this poleward eddy transport can be associated with tropical

systems and with tropical extratropical interaction. This is consistent with the discussion of Grise and Thompson (2012). Filaments emanating from the top of deep convective towers can turn eastward and reach deep into the winter subtropics where they may interact with the weather systems on the subtropical jet to enhance their poleward fluxes of angular momentum. Evidence for this idea was given in  $\text{HC}_{\text{JJA}}$  and  $\text{HC}_{\text{DJF}}$ , and it is strongly supported by the joint probability distributions for tropical OLR and the lagged momentum flux at  $20^{\circ}\text{S}$  presented in Fig. 6 and summarized in Table 1. It is also supported by the diagnostics discussed in section 5 which show the impact on synoptic time scales of summer tropical deep convection on the strength of the winter STJ, and that this impact is largest in the longitudinal ranges of the deep convection.

The tilt of the upper-tropospheric cross-equatorial flows into the winter hemisphere, northeast–southwest in JJA, northwest–southeast in DJF, imply for these seasons the momentum transports out of the winter hemisphere. Yang et al. (2007b, Fig. 5) showed this to be a characteristic of the flow structure associated with westward-moving deep convection in the northern tropics in JJA, and that a significant portion of it is described by projections on to the meridional mode number  $n = 0$  [mixed Rossby–gravity (MRG)] and  $n = 1$  (Rossby) equatorial wave modes. The lower tropospheric structure is dominated by a Rossby wave structure in the summer tropical region, and this appears to provide the organization there for the deep convection and upper-tropospheric flow development. The importance of westward-moving MRGs (WMRGs) in the upper troposphere was also highlighted in  $\text{HC}_{\text{JJA}}$  and  $\text{HC}_{\text{DJF}}$ , and for the Hadley cell in the North Atlantic in DJF it was noted by Tomassini and Yang (2022).

Important questions are “why is there a horizontal tilt in the cross-equatorial flow into the winter hemisphere?” and “is the tilt related to the fact that the deep convection is in the summer hemisphere?” The tilt does correspond to that required for meridional propagation of barotropic Rossby wave activity from the summer tropics into the winter hemisphere (e.g., Hoskins and Karoly 1981). In the perspective of Charney (1963) this barotropic result would perhaps be seen as applicable in the upper troposphere in the tropics. The momentum flux into the hemisphere in which wave activity is forced is consistent with that expected from transformed Eulerian mean theory (Andrews and McIntyre 1978).

For equatorially trapped Rossby waves, with discrete meridional structures, a straightforward group velocity argument is not possible. However, meridional group velocity for plane waves can be envisaged by considering the time development from an initial state composed of waves with the same wavelength in  $x$  but neighboring wavelengths in  $y$ , adding to give a local structure in  $y$ . Based on this idea, Fig. 13a shows an initial state that is a superposition of the two wavenumber-6 equatorial Rossby-like modes with the gravest latitudinal structures, the  $n = 0$  WMRG and the  $n = 1$  Rossby equatorial waves. The wave structures (and other details) are as in Yang et al. (2007a, Fig. 1). At day 0 (Fig. 13a), the phases of the waves are identical, and the relative amplitudes chosen so that their combination gives strong reinforcement in the



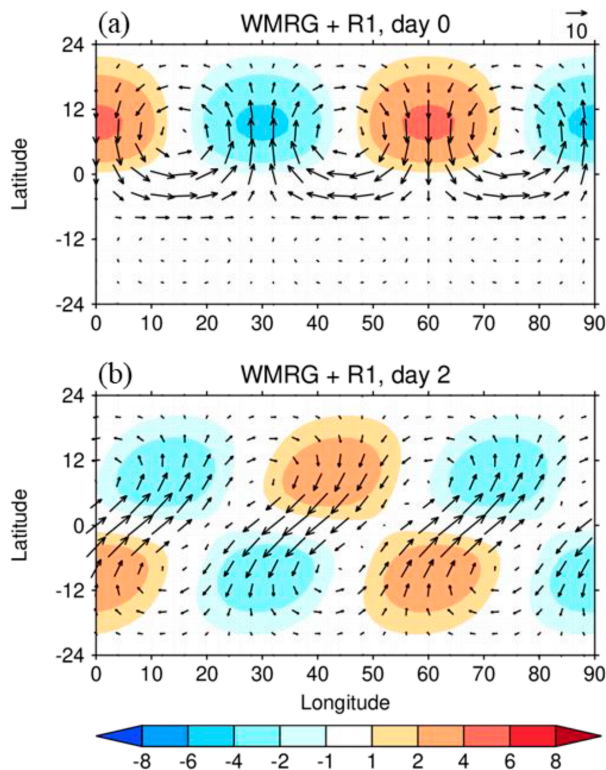


FIG. 13. A superposition of two free equatorial wave modes at day 0 and the development by day 2. Vectors indicate horizontal wind and colors indicate divergence. The two waves are the gravest modes in the latitudinal direction, the  $n = 0$  Westward-moving mixed Rossby–gravity (WMRG) wave and the  $n = 1$  Rossby (R1) wave. Both have zonal wavenumber 6. The structures of the individual waves are shown in Fig. 1 of Yang et al. (2007a), and the choices of the zonal scale and the equatorial trapping scale of  $6^\circ$  are justified from analysis of observational data in Yang et al. (2012). The relative amplitudes of the two waves are chosen so that the magnitudes of their meridional winds are identical at  $8.5^\circ\text{N/S}$ , the latitudes at which the R1 wave meridional wind has its maximum. The phases of the two waves at day 0 are identical, and the day 2 picture is obtained by superposition of the two waves, each having moved westward with its own phase speed:  $15\text{ m s}^{-1}$  for the WMRG and  $6\text{ m s}^{-1}$  for the R1. The amplitude of the pattern is arbitrary, but if the arrow at the top right represents  $10\text{ m s}^{-1}$ , then the unit for divergence is  $10^{-6}\text{ s}^{-1}$ .

Northern Hemisphere and near cancellation in the Southern Hemisphere. The divergence associated with both waves has a maximum in the Northern Hemisphere in the longitude of the strongest northerly winds. This can be envisaged as a wave coupled with strong deep convection occurring in this divergence region in the tropics north of the equator. Using the theoretical dispersion relations for linear waves in a resting atmosphere, the WMRG propagates much more rapidly westward ( $15\text{ m s}^{-1}$ ) than the  $n = 1$  Rossby wave ( $6\text{ m s}^{-1}$ ), and this leads to the flow structure shown in Fig. 13b. The development of a strong northeast–southwest-tilted cross-equatorial flow in the 2-day period, and the similarity with the upper-tropospheric structures shown in Yang et al. (2007b,

Fig. 5a) and  $\text{HC}_{\text{JJA}}$  are striking. This strongly supports the view that upper-tropospheric wave activity associated with deep tropical convection in the summer hemisphere preferentially propagates across the equator into the winter hemisphere and that, associated with this, there is tilted cross-equatorial flow and a transfer of momentum from the winter hemisphere to the summer hemisphere.

The importance of transient near-equatorial waves for Hadley cell behavior, and in their organization of convection in the tropical region is consistent with a wide range of aquaplanet GCM experiments. For a standard, equatorially symmetric SST profile, Blackburn et al. (2013) summarized the large range of near-equatorial precipitation, equatorial wave and Hadley cell behavior given by 16 atmospheric models developed by major climate modeling centers. Following the initial study of Sumi (1992), many papers have investigated the weak Hadley cells formed when uniform SST is imposed. Horinouchi (2012) stressed the importance of equatorial waves for organizing a convective maximum in the equatorial region and, consequently, for the weak Hadley cell associated with it. This remained the case even when pole to equator SST gradients were included.

It is hoped that this paper will stimulate further investigations of variability on synoptic to intraseasonal time scales in the tropics, its interaction with variability in higher latitudes, and the importance in the general circulation. The realism of the representation of these processes in weather and climate models will also be important to assess.

**Acknowledgments.** G-YY was supported by the National Centre for Atmospheric Science through the NERC National Capability International Programmes Award (NE/X006263/1). The authors would like to acknowledge the input of three reviewers and the editor, which has significantly improved the paper. BH would also like to acknowledge extremely fruitful discussions with Professor J. M. Wallace.

**Data availability statement.** The ERA-Interim data (Dee et al. 2011) are generated by ECMWF and distributed by the Climate Data Store (CDS), under the Copernicus Climate Change Service (C3S). The OLR data (Liebmann and Smith 1996) are available at [https://psl.noaa.gov/data/gridded/data.interp\\_OLR.html](https://psl.noaa.gov/data/gridded/data.interp_OLR.html). Computing and data storage facilities were provided by JASMIN (<https://jasmin.ac.uk>).

## REFERENCES

- Andrews, D. G., and M. E. McIntyre, 1978: An exact theory of nonlinear waves on a Lagrangian-mean flow. *J. Fluid Mech.*, **89**, 609–646, <https://doi.org/10.1017/S0022112078002773>.
- Blackburn, M., and Coauthors, 2013: The Aqua-Planet Experiment (APE): Control SST simulations. *J. Meteor. Soc. Japan*, **91A**, 17–56, <https://doi.org/10.2151/jmsj.2013-A02>.
- Charney, J. G., 1963: A note on large-scale motions in the tropics. *J. Atmos. Sci.*, **20**, 607–609, [https://doi.org/10.1175/1520-0469\(1963\)020<0607:ANOLSM>2.0.CO;2](https://doi.org/10.1175/1520-0469(1963)020<0607:ANOLSM>2.0.CO;2).
- Dee, D. P., and Coauthors, 2011: The ERA-Interim reanalysis: Configuration and performance of the data assimilation



- system. *Quart. J. Roy. Meteor. Soc.*, **137**, 553–597, <https://doi.org/10.1002/qj.828>.
- Dima, I. M., J. M. Wallace, and I. Kraucunas, 2005: Tropical zonal momentum balance in the NCEP reanalyses. *J. Atmos. Sci.*, **62**, 2499–2513, <https://doi.org/10.1175/JAS3486.1>.
- Grise, K. M., and D. W. J. Thompson, 2012: Equatorial planetary waves and their signature in atmospheric variability. *J. Atmos. Sci.*, **69**, 857–874, <https://doi.org/10.1175/JAS-D-11-0123.1>.
- Held, I. M., 2000: The general circulation of the atmosphere. *Proc. Program in Geophysical Fluid Dynamics*, Woods Hole, MA, Woods Hole Oceanographic Institution, 54 pp., [https://gfd.whoi.edu/wp-content/uploads/sites/18/2018/03/lectures2000\\_21464.pdf](https://gfd.whoi.edu/wp-content/uploads/sites/18/2018/03/lectures2000_21464.pdf).
- , 2019: 100 years of progress in understanding the general circulation of the atmosphere. *A Century of Progress in Atmospheric and Related Sciences: Celebrating the American Meteorological Society Centennial*, Meteor. Monogr., No. 59, Amer. Meteor. Soc., 6.1–6.23, <https://doi.org/10.1175/AMSMONOGRAPHS-D-18-0017.1>.
- , and A. Y. Hou, 1980: Nonlinear axially symmetric circulations in a nearly inviscid atmosphere. *J. Atmos. Sci.*, **37**, 515–533, [https://doi.org/10.1175/1520-0469\(1980\)037<0515:NASCIA>2.0.CO;2](https://doi.org/10.1175/1520-0469(1980)037<0515:NASCIA>2.0.CO;2).
- Horinouchi, T., 2012: Moist Hadley cell circulation: Possible role of wave–convection coupling in aquaplanet experiments. *J. Atmos. Sci.*, **69**, 891–907, <https://doi.org/10.1175/JAS-D-11-0149.1>.
- Hoskins, B. J., and D. J. Karoly, 1981: The steady linear response of a spherical atmosphere to thermal and orographic forcing. *J. Atmos. Sci.*, **38**, 1179–1196, [https://doi.org/10.1175/1520-0469\(1981\)038<1179:TSLROA>2.0.CO;2](https://doi.org/10.1175/1520-0469(1981)038<1179:TSLROA>2.0.CO;2).
- , and G.-Y. Yang, 2021: The detailed dynamics of the Hadley cell. Part II: December–February. *J. Climate*, **34**, 805–823, <https://doi.org/10.1175/JCLI-D-20-0504.1>.
- , H.-H. Hsu, I. N. James, M. Masutani, P. D. Sardeshmukh, and G. H. White, 1989: Diagnostics of the global atmospheric circulation based on ECMWF analyses 1979–1989. World Meteorological Organization WMO/TD 326/WCRP-27, 217 pp., [https://library.wmo.int/doc\\_num.php?explnum\\_id=9517](https://library.wmo.int/doc_num.php?explnum_id=9517).
- , G.-Y. Yang, and R. M. Fonseca, 2020: The detailed dynamics of the June–August Hadley cell. *Quart. J. Roy. Meteor. Soc.*, **146**, 557–575, <https://doi.org/10.1002/qj.3702>.
- Kraucunas, I., and D. L. Hartmann, 2005: Equatorial superrotation and the factors controlling the zonal-mean zonal winds in the tropical upper troposphere. *J. Atmos. Sci.*, **62**, 371–389, <https://doi.org/10.1175/JAS-3365.1>.
- Lee, S., 1999: Why are the climatological zonal winds easterly in the equatorial upper troposphere? *J. Atmos. Sci.*, **56**, 1353–1363, [https://doi.org/10.1175/1520-0469\(1999\)056<1353:WATCZW>2.0.CO;2](https://doi.org/10.1175/1520-0469(1999)056<1353:WATCZW>2.0.CO;2).
- Liebmann, B., and C. A. Smith, 1996: Description of a complete (interpolated) outgoing longwave radiation dataset. *Bull. Amer. Meteor. Soc.*, **77**, 1275–1277, <https://doi.org/10.1175/1520-0477-77.6.1274>.
- Lindzen, R. S., and A. V. Hou, 1988: Hadley circulations for zonally averaged heating centered off the equator. *J. Atmos. Sci.*, **45**, 2416–2427, [https://doi.org/10.1175/1520-0469\(1988\)045<2416:HCFZAH>2.0.CO;2](https://doi.org/10.1175/1520-0469(1988)045<2416:HCFZAH>2.0.CO;2).
- Randel, W. J., and I. M. Held, 1991: Phase speed spectra of transient eddy fluxes and critical layer absorption. *J. Atmos. Sci.*, **48**, 688–697, [https://doi.org/10.1175/1520-0469\(1991\)048<0688:PSSOTE>2.0.CO;2](https://doi.org/10.1175/1520-0469(1991)048<0688:PSSOTE>2.0.CO;2).
- Riehl, H., 1950: On the role of the tropics in the general circulation of the atmosphere. *Tellus*, **2**, 1–17, <https://doi.org/10.3402/tellusa.v2i1.8531>.
- , and J. S. Malkus, 1958: On the heat balance in the equatorial trough zone. *Geophysica*, **6**, 503–537.
- Schneider, E. K., 1977: Axially symmetric steady-state models of the basic state for instability and climate studies. Part II. Nonlinear calculations. *J. Atmos. Sci.*, **34**, 280–296, [https://doi.org/10.1175/1520-0469\(1977\)034<0280:ASSSMO>2.0.CO;2](https://doi.org/10.1175/1520-0469(1977)034<0280:ASSSMO>2.0.CO;2).
- Schneider, T., 2006: The general circulation of the atmosphere. *Rev. Earth Planet. Sci.*, **34**, 655–688, <https://doi.org/10.1146/annurev.earth.34.031405.125144>.
- Simmons, A. J., and H. J. Hoskins, 1980: Barotropic influences on the growth and decay of nonlinear baroclinic waves. *J. Atmos. Sci.*, **37**, 1679–1684, [https://doi.org/10.1175/1520-0469\(1980\)037<1679:BIOTGA>2.0.CO;2](https://doi.org/10.1175/1520-0469(1980)037<1679:BIOTGA>2.0.CO;2).
- Starr, V. P., 1948: An essay on the general circulation of the Earth's atmosphere. *J. Meteor.*, **5**, 39–43, [https://doi.org/10.1175/1520-0469\(1948\)005<0039:AEOTGC>2.0.CO;2](https://doi.org/10.1175/1520-0469(1948)005<0039:AEOTGC>2.0.CO;2).
- Sumi, A., 1992: Pattern formation of convective activity over the aqua-planet with globally uniform Sea Surface Temperature (SST). *J. Meteor. Soc. Japan*, **70**, 855–876, [https://doi.org/10.2151/jmsj1965.70.5\\_855](https://doi.org/10.2151/jmsj1965.70.5_855).
- Thorncroft, C. D., B. J. Hoskins, and M. E. McIntyre, 1993: Two paradigms of baroclinic-wave life-cycle behavior. *Quart. J. Roy. Meteor. Soc.*, **119**, 17–55, <https://doi.org/10.1002/qj.49711950903>.
- Tomassini, L., and G.-Y. Yang, 2022: Tropical moist convection an important driver of Atlantic Hadley circulation variability. *Quart. J. Roy. Meteor. Soc.*, **148**, 3287–3302, <https://doi.org/10.1002/qj.4359>.
- Walker, C. C., and T. Schneider, 2006: Eddy influences on Hadley circulations: Similarity with an idealized GCM. *J. Atmos. Sci.*, **63**, 3333–3350, <https://doi.org/10.1175/JAS3821.1>.
- Yang, G.-Y., B. Hoskins, and J. Slingo, 2007a: Convectively coupled equatorial waves. Part I: Horizontal and vertical structures. *J. Atmos. Sci.*, **64**, 3406–3423, <https://doi.org/10.1175/JAS4017.1>.
- , —, and —, 2007b: Convectively coupled equatorial waves. Part III: Synthesis structures and their forcing and evolution. *J. Atmos. Sci.*, **64**, 3438–3451, <https://doi.org/10.1175/JAS4019.1>.
- , —, and L. Gray, 2012: The influence of the QBO on the propagation of equatorial waves into the stratosphere. *J. Atmos. Sci.*, **69**, 2959–2982, <https://doi.org/10.1175/JAS-D-11-0342.1>.